การวิเคราะห์โครงสร้างของไทเทเนียมไทรอะลูมิไนด์ที่มีอะตอม
ของแมงกานีส 6.2 เปอร์เซ็นต์โดยปริมาณ

นายยุทธพงษ์ อินทร์กง

STRUCTURAL CHARACTERIZATIONS OF TITANIUM

TRIALUMINIDE WITH 6.2 ATOMIC PERCENT

MANGANESE

Mr. Yutthapong Inkong

STRUCTURAL CHARACTERIZATIONS OF TITANIUM

TRIALUMINIDE WITH 6.2 ATOMIC PERCENT

MANGANESE

Suranaree University of Technology has approved this thesis submitted in partial fulfillment of the requirements for a Master's Degree.

Thesis Examining Committee
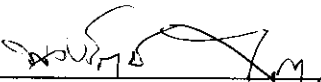
_____

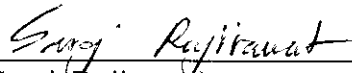(Assoc. Prof. Dr. Sukit Limpijumnong)

Chairperson

_____

(Asst. Prof. Dr. Prapun Manyum)
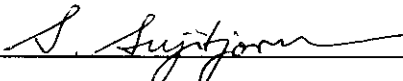
Member (Thesis Advisor)

_____

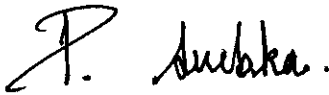(Asst. Prof. Dr. Puangratana Pairor)

Member

_____

(Dr. Saroj Rujirawat)

Member

_____   _____

(Assoc. Prof. Dr. Sarawut Sujitjorn)   (Assoc. Prof. Dr. Prasart Suebka)

Vice Rector for Academic Affairs   Dean of Institute of Science

ยุทธพงษ์ อินทร์กง : การวิเคราะห์โครงสร้างของไทเทเนียมไทรอะลูมิไนด์ที่มีอะตอม
ของแมงกานีส 6.2 เปอร์เซ็นต์โดยปริมาณ (STRUCTURAL CHARACTERIZATIONS
OF TITANIUM TRIALUMINIDE WITH 6.2 ATOMIC PERCENT MANGANESE)
อาจารย์ที่ปรึกษา : ผู้ช่วยศาสตราจารย์ ดร.ประพันธ์ แม่นยำ, 42 หน้า.

ISBN 974-533-418-9

ได้ปลูกผลึกเดี่ยวของไทเทเนียมไทรอะลูมิไนด์ ที่ดัดแปรให้มีโครงสร้างแบบ $L1_2$ ซึ่งมี
อะตอมของแมงกานีส 6.2 เปอร์เซ็นต์โดยปริมาณ โดยวิธีโซนลอย ได้ศึกษาโครงสร้างระดับ
ไมครอนและองค์ประกอบทางเคมีของผลึก โดยใช้กล้องจุลทรรศน์อิเล็กตรอนแบบส่องผ่าน กล้อง
จุลทรรศน์อิเล็กตรอนแบบส่องกราด กล้องจุลทรรศน์เชิงแสง เครื่องเอกซ์เรย์ดิฟแฟรกโทมิเตอร์
และเครื่องอิเล็กตรอนไมโครโพรบอนาไลเซอร์ การศึกษาโดยใช้กล้องจุลทรรศน์อิเล็กตรอนแบบ
ส่องกราดไม่พบอนุภาคเฟสอื่น พบเฉพาะรูพรุน อย่างไรก็ตาม จากการสังเกตโดยใช้กล้อง
จุลทรรศน์อิเล็กตรอนแบบส่องผ่าน พบว่า มีอนุภาคของ $TiAl_2$ ที่มีโครงสร้างแบบ Ga_2Hf มี
ลักษณะคล้ายจานวางตัวอยู่ตามระนาบ {100} ของผลึก

สาขาวิชาฟิสิกส์   ลายมือชื่อนักศึกษา _____

ปีการศึกษา 2547   ลายมือชื่ออาจารย์ที่ปรึกษา _____

YUTTHAPONG INKONG : STRUCTURAL CHARACTERIZATIONS OF
TITANIUM TRIALUMINIDE WITH 6.2 ATOMIC PERCENT
MANGANESE. THESIS ADVISOR : ASST. PROF. PRAPUN MANYUM,
Ph.D. 42 PP. ISBN 974-533-418-9

SINGLE CRYSTAL/TITANIUM TRIALUMINIDE/MANGANESE-MODIFIED/
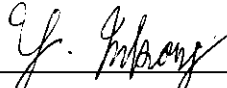MICROSTRUCTURE/PRECIPITATES
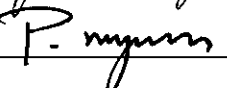
Single crystal of 6.2 atomic% Mn-modified $TiAl_3$ with $L1_2$ ordered structure
was grown by floating zone technique. The microstructure and chemical composition
of the crystal were studied by using a transmission electron microscope, scanning
electron microscope, optical microscope, X-ray diffractometer and electron
microprobe analyzer. No second phase precipitates were observed under scanning
electron microscope investigation. Only pores were observed. Transmission electron
microscope observation revealed that there were plate-like precipitates of $TiAl_2$ with
Ga_2Hf type structure lying along the {100} planes of the matrix.

School of Physics

Academic Year 2004

Student's Signature _____

Advisor's Signature _____

ACKNOWLEDGEMENTS

This thesis could not have been completed without the help and support of many people. I would like to thank :

- Asst. Prof. Dr. Prapun Manyum, my thesis advisor, for his patient guidance, kindness and encouragement throughout my study.

- Professor Glyn Taylor, Department of Materials, University of Oxford, for his assistance in the growth of single crystal for this study and some characterization.

- Asst. Prof. Dr. Puangratana Pairor, for her taking her time to edit this thesis.

- Assoc. Prof. Dr. Prasart Suebka, my teacher, for his kindness and help.

- Mr. Sangphet Ngonchaiyaphum, Mr. Anuchit Ruangvittayanon, Ms. Janjira Rujirawat, Ms. Nongnaphat Khosavithitkul and Ms. Korawan Ratanachai, who work at the Center for Scientific and Technological Equipment, Suranaree University of Technology, for their help in operating equipment during specimen characterization.

- All staff members of the Institute of Science, Suranaree University of Technology, for their hospitality.

- All graduate students at the School of Physics, Suranaree University of Technology, between the years 2000 and 2004 for being my good friends.

Finally, I would like to express my gratitude to my parents and my sisters for their understanding, encouragement and support throughout my studies.

<div align="right">Yutthapong Inkong</div>

CONTENTS

CONTENTS (Continued)

LIST OF TABLES

LIST OF FIGURES

LIST OF FIGURES (Continued)

LIST OF ABBREVIATIONS

TEM   =   Transmission Electron Microscope

SEM   =   Scanning Electron Microscope

SAD   =   Selected Area Diffraction

BF   =   Bright Field

DF   =   Dark Field

B   =   Beam direction

f.c.c.   =   Face Center Cubic

at.%   =   Atomic percent

CHAPTER I

INTRODUCTION AND LITERATURE REVIEW

Intermetallic compounds are formed by combination of various metals in suitable amounts. The properties and the crystal structures of intermetallics are different from those of the constituent metals (Sauthoff, 1995). During the last few decades, intermetallics have been of enormous interest. The Intermetallic compound $TiAl_3$ has attracted attention because of its low density (its density of 3.3 g/cm^3 is lower than that of Ti_3Al and $TiAl$), high melting point and an oxidation resistance (Nakayama and Mabuchi, 1993; Shirai, Masaki, and Yamakuchi, 1994; Bohnenkamp, Wang, Jeweet, and Dahms, 1994 ; Douin, Sharvan Kumar, and Veyssiere, 1995 ; Fukunaka, Kolba, Yamada, and Miura, 1997; Tian and Nemoto, 1997; Pettifor, 1993) that is significantly higher than that of the other titanium aluminides. Thus $TiAl_3$ is a candidate phase for lightweight structural applications and use in aerospace applications. It is also being considered as a coating material. However, it has a low-symmetry tetragonal $D0_{22}$ structure (Fig.1.1(a)) and is brittle at room temperature, making it unsuitable for some applications. A material fractures in a brittle manner if there is no plastic deformation. The reason for this may be an insufficient number of slip systems. It was found that by addition of somewhat transition elements such as Cr, Mn, Fe, Co and Ni (Sauthoff, 1995; Nakayama and Mabuchi, 1993; Shirai et al., 1994; Bohnenkamp et al., 1994; Douin et al., 1995; Fukunaka et al., 1997; Kogachi and Kameyama, 1995; Nic and Mikkola, 1999; Tian and Nemoto, 2000a; 2000b;

Mabuchi, Kito, Nakamoto, Tsuda, and Nakayama, 1996) that the low symmetry tetragonal $D0_{22}$ structure can be transformed into the high symmetry cubic $L1_2$ structure (Fig. 1.1(b)) by displacing every (001) plane by a $\frac{1}{2}[110]$ vector. The cubic $L1_2$ structure has the requisite five independent slip systems for homogeneous deformation. The tetragonal $D0_{22}$ structure is derived from the cubic $L1_2$ structure by displacing Al atom position by an additional transition element.
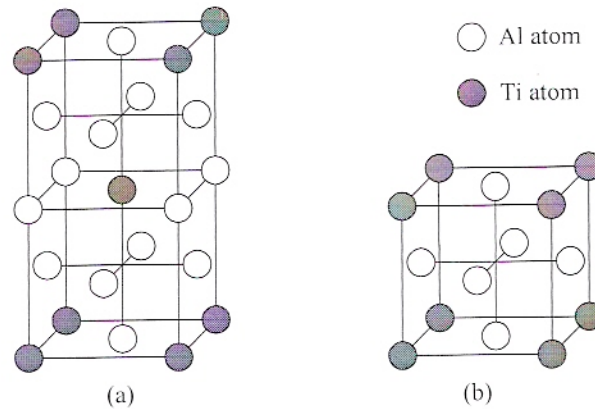
Figure 1.1 (a) $D0_{22}$ and (b) $L1_2$ structures.

Figure 1.2 shows the predicted heat of formation of different ordered structures of titanium-aluminides (Pettifor, 1993). As indicated by an arrow, the cubic $L1_2$ phase is very close to the ground state energy of the tetragonal $D0_{22}$ $TiAl_3$. It was found that the $L1_2$ structure can be stabilised by addition of transition elements (Sauthoff, 1995; Nakayama and Mabuchi, 1993; Shirai et al., 1994; Bohnenkamp et al., 1994; Douin et al., 1995; Fukunaka et al., 1997). Since $L1_2$ is cubic, there are more slip systems available during plastic deformation than for the $D0_{22}$ structure; it is hoped that the new compound might be more ductile.
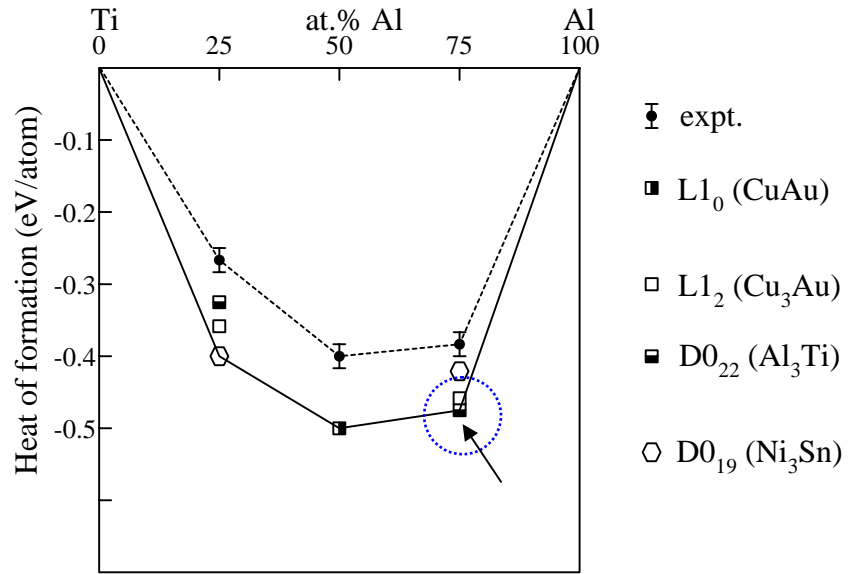
Figure 1.2 The predicted heat of formation of titanium-aluminium compounds.

The studies on $TiAl_3$ with $L1_2$ structure have been carried out by several groups. Kogachi and Kameyama (1995) studied site occupancies by Cr in the $L1_2$ compound $TiAl_3$. The lattice constant is found to steadily increase with an increase in Ti-content for 9, 11 and 13% Cr alloys. Changes in the lattice constant may be explained by the atomic size effect, i.e. the replacement of smaller Al atoms by larger Ti atoms.

The authors also found that the occupation of the Al-site by Al atoms decreases linearly with the increase in Ti and Cr contents. Some Al atoms are substituted on the Ti-sites. In ternary $L1_2$ alloy, ternary atoms usually occupy the Al-site when the Ti content is low. However at 13% Cr, some Cr atoms also occupy the Ti-sites. The defect that is caused by ternary atoms occupying the host atom sites is called the antisite defect.

Nic and Mikkola (1999), who studied the site occupancy in cubic $TiAl_3$-Cr alloy using an X-ray diffraction method, found a small amount of Cr substitution, but no Al substitution, on the Ti-sites, and observed that most of the Cr atoms are on the Al-sites. Increasing number of Cr causes more Cr to occupy the Ti-sites, displacing some Ti atoms to the Al-sites, thus creating more antisite defects. The antisite defects are the primary point defects in cubic $L1_2$ ordered alloys, constitutional vacancies are not important. However defects can influence mechanical properties of intermetallic alloys.

Tian and Nemoto (1997, 2000a, 2000b) studied Ag-modified cubic $L1_2$-$TiAl_3$, which contains second phases consisting of tetragonal $L1_0$-TiAl(Ag) and $D0_{23}$-Ti_5Al_{11} structures, respectively. They found that for alloys containing the $L1_0$-TiAl(Ag) second phase, the crystal structures of $L1_0$-TiAl(Ag) and $L1_2$-$Ti(Al,Ag)_3$ are both based on the f.c.c. structure. The lattice misfits are anisotropic in [100], [010] and [001] directions due to the tetragonal structure of $L1_0$-TiAl(Ag) precipitate. The lattice parameters of $L1_0$-TiAl(Ag) and $L1_2$-$Ti(Al,Ag)_3$ were measured, using X-ray powder diffraction method, in order to determine the lattice misfit between the precipitate and matrix. The measured lattice parameters are a = 0.3995 nm and c = 0.4063 nm for $L1_0$-TiAl(Ag) phase and a = 0.4003 nm for the $L1_2$-$Ti(Al,Ag)_3$.

The growth of $L1_0$-TiAl(Ag) precipitates is restrained in the [001] direction of the $L1_2$ matrix due to the larger misfit in this direction and this leads to a morphology of plate-like precipitates parallel to the {001} planes of the matrix lattice at initial aging time. The orientation relationship between the $L1_0$-TiAl(Ag) precipitates and

the $L1_2$-Ti(Al,Ag)$_3$ matrix is described as $(001)_p//(001)_m$, $[100]_p//[100]_m$, where m denotes the $L1_2$-Ti(Al,Ag)$_3$ matrix and p denotes the $L1_0$-TiAl(Ag) precipitates.

Microstructure development during aging in such alloy system was found to be mainly controlled by coherency stresses across the precipitate/matrix interface. Although the linear elastic theory can explain the deviation of the habit plane from {001}, the surface energy and interaction between precipitates are also important factors affecting the precipitate morphology.

For alloys containing the $D0_{23}$-Ti$_5$Al$_{11}$ second phase, the measured lattice parameters are a = 0.3993 nm for the $L1_2$-Ti(Al,Ag)$_3$ matrix and a = 0.3917 nm and c = 0.4131 nm for $D0_{23}$-Ti$_5$Al$_{11}$ phase. By TEM observation and a comparison of the observed results with the prediction of the linear elastic theory, the $D0_{23}$-Ti$_5$Al$_{11}$ precipitates formed in $L1_2$-Ti(Al,Ag)$_3$ matrix during aging has a thin-plate multi-domain morphology. The multi-domain structures look like a sandwich composed of regularly spaced alternating thin {110} layers.

The habit plane of the thin plates which make up the multi-domain structures of the $D0_{23}$-Ti$_5$Al$_{11}$ precipitates is {110} type of the $L1_2$ matrix. The multi-domain structures can be considered as twin structures with the tetragonal axis of the twin I parallel to the [100] direction and that of twin II parallel to the [010] direction of the matrix. The relative orientation of the $D0_{23}$-Ti$_5$Al$_{11}$ precipitates and the $L1_2$-Ti(Al,Ag)$_3$ matrix is described as $(100)_{Ip}//(001)_m$, near $[001]_{Ip}//[100]_m$, $(100)_{IIp}//(001)_m$, near $[001]_{IIp}//[010]_m$, where Ip and IIp denote $D0_{23}$-Ti$_5$Al$_{11}$ precipitates for twin I and twin II, respectively, and m denotes the $L1_2$-Ti(Al,Ag)$_3$ matrix.

Mabushi et al. (1996), who investigated the effects of manganese on the formation of the ternary $L1_2$ compound in $TiAl_3$-based alloys, found that there were many types of second phases possible in the $L1_2$ matrix depending on the amount of Mn concentration. These phases are TiAl, $TiAl_2$, Ti_2Al_5, $TiAl_3$, Al_8Mn_5 and TiAlMn. Porosity was observed together with the Al_8Mn_5 phases after homogenization. However there was no porosity when the TiAlMn phases are formed. It was found that the ternary $L1_2$ phase containing Mn had some bend ductility at room temperature. The studies of dislocation structure in polycrystalline $L1_2$ Mn-modified $TiAl_3$ deformation shows no superlattice intrinsic stracking fault couple dislocations. This confirms that in Mn-modified $TiAl_3$ superdislocations are antiphase boundary-couple.

The $TiAl_2$ has a 1-dimensional antiphase domain structure (1d-APS) of the Ga_2Hf type base on $L1_2$ structure was observed by Miida (1986). The characteristic feature of the electron diffraction pattern of the $TiAl_2$ phase is the appearance of two orthogonal sets of small satellite spots around the diffracted spots of the matrix. The $TiAl_2$ compound with the Ga_2Hf type structure was confirmed by the study of Wu and Pope (1994). The $TiAl_2$ precipitates have a thin plate-like structure lying parallel to the cube planes of the $L1_2$ matrix.

From the study of Manyum and Taylor (2002), an addition of 10 at.%Mn into $TiAl_3$, the $D0_{22}$ structure is transformed to the $L1_2$ structure by ~70% and an unidentified second phase with dendritic structure occur (Fig. 1.3). This may be due to an excessive concentration of Mn. From X-ray analysis the second phase is seen to

consist mainly of Mn and some Al. Some porosity was observed. In addition, the material is found to be very brittle and it is difficult to prepare samples for characterization. In their study, polycrystalline sample were used.
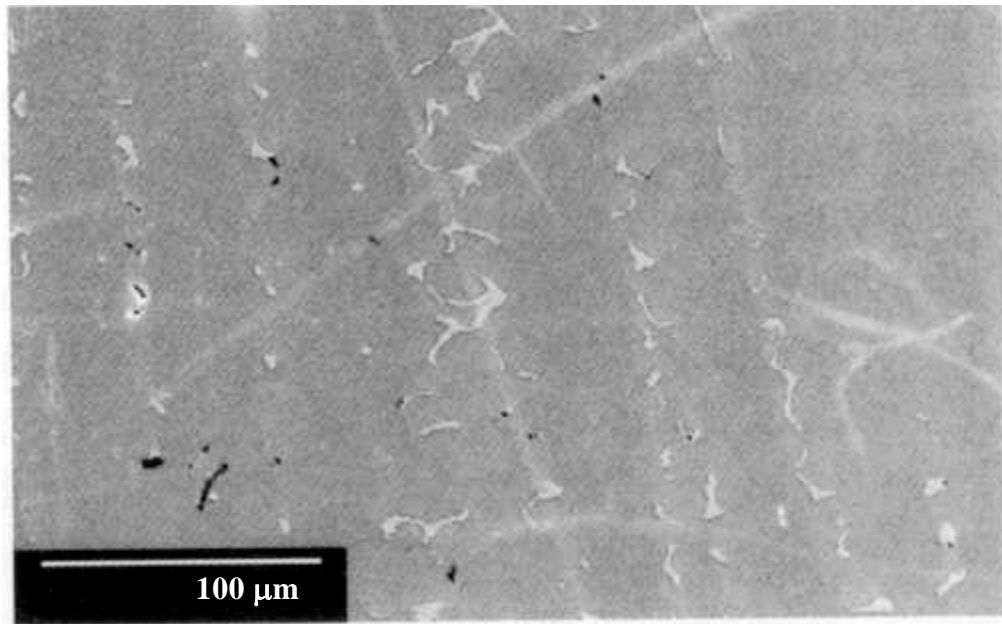
Figure 1.3 SEM micrograph showing second phases.

The objective of this study is to try to change the structure of $TiAl_3$ from $D0_{22}$ to $L1_2$. It is hoped that the addition of about 7 at.%Mn will eliminate the second phase from the system. The structure, along with the micro- and nanostructure of the new compound will be studied. It is also hoped that the material will be more ductile. Single crystal of $TiAl_3$-Mn will be used because second phase precipitates in single crystal specimens were usually more easily to recognize than those in polycrystalline materials. The disordering of the $TiAl_3$-Mn crystal is studied using a ball milling process.

CHAPTER II

EXPERIMENTAL PROCEDURE

2.1 Preparation of single crystal

2.1.1 Feed material preparation

The starting material was taken from a button ingot, 25 at.%Ti, 65 at.%Al, 10 at.%Mn nominal composition supplying by TIMET UK Limited. Its microstructure and chemical composition were studied by Manyum and Taylor (2002). Their study suggests that reduction of Mn to about 7 at.% may cause the second phase to disappear. Therefore a new composition alloy was prepared for this study.

Initially, a new compound of 25 at.%Ti, 68 at.%Al, 7 at.%Mn was prepared from the alloy mentioned above by addition of high purity Ti and Al to reduced the concentration of Mn to about 7 at.%. The combination was then mixed using a ball milling process and subsequently arc-melted to make a new composition alloy. The alloy was triple melted in Ar atmosphere to reduce inhomogeneities and possibility of cracking. It is a polycrystalline material with a rod shape of about 70 mm long and non-uniform diameter of about 10 mm along the rod. The material was then chemically polished to remove any surface impurities. This material was used as a feed material for growing single crystal.

Since no particular orientation of $TiAl_3$ single crystal was preferable, for convenience a single crystal of TiAl with approximately 6 mm diameter available in the laboratory was used as a seed crystal. The axial orientation of the TiAl crystal was

near the [001] direction. The orientation was determined using the Laue X-ray method.

2.1.2 Crystal growth

A single crystal was grown using a NEC SCN35HD Image Furnace, which enables a crystal to be produced by the floating zone technique at the Department of Materials, University of Oxford. Figure 2.1 shows a schematic diagram of the apparatus. A single crystal is formed when a polycrystalline feed rod is melted and solidified in a controlled manner by passing a molten zone slowly along the length of the bar. The orientation of solidified material is controlled by the seed which is a single rod of known orientation. A molten zone is produced by focusing radiation from two halogen lambs using two gold-plated ellipsoidal reflecting mirrors. The feed and seed materials are attached to upper and lower vertically shafts respectively, which move up and down a common axis through the operation of a harmonic drive system and enable the material to be a positioned at the foci of the reflecting mirrors. The material can be melted when radiation from the lamps is sufficient. The growth process occurs inside a quartz tube that can be pumped down to 1×10^{-6} mbar using a turbo molecular vacuum pump backed by a rotary pump, thus, growth can be carried out in a vacuum or in a gaseous atmosphere. A video camera and TV monitor are used to view the molten zone during growth single crystal.

The feed material was suspended from the upper shaft by spark-drilling a hole with 1 mm diameter through the top of the feed bar and inserting a Mo rod through the hole. Mo wire is then attached to the rod to form a loop allowed the feed bar to be simply hung from a hook screwed to the shaft. Seed was held in a ceramic holder

which screwed into the lower shaft via a stainless steel holding piece.
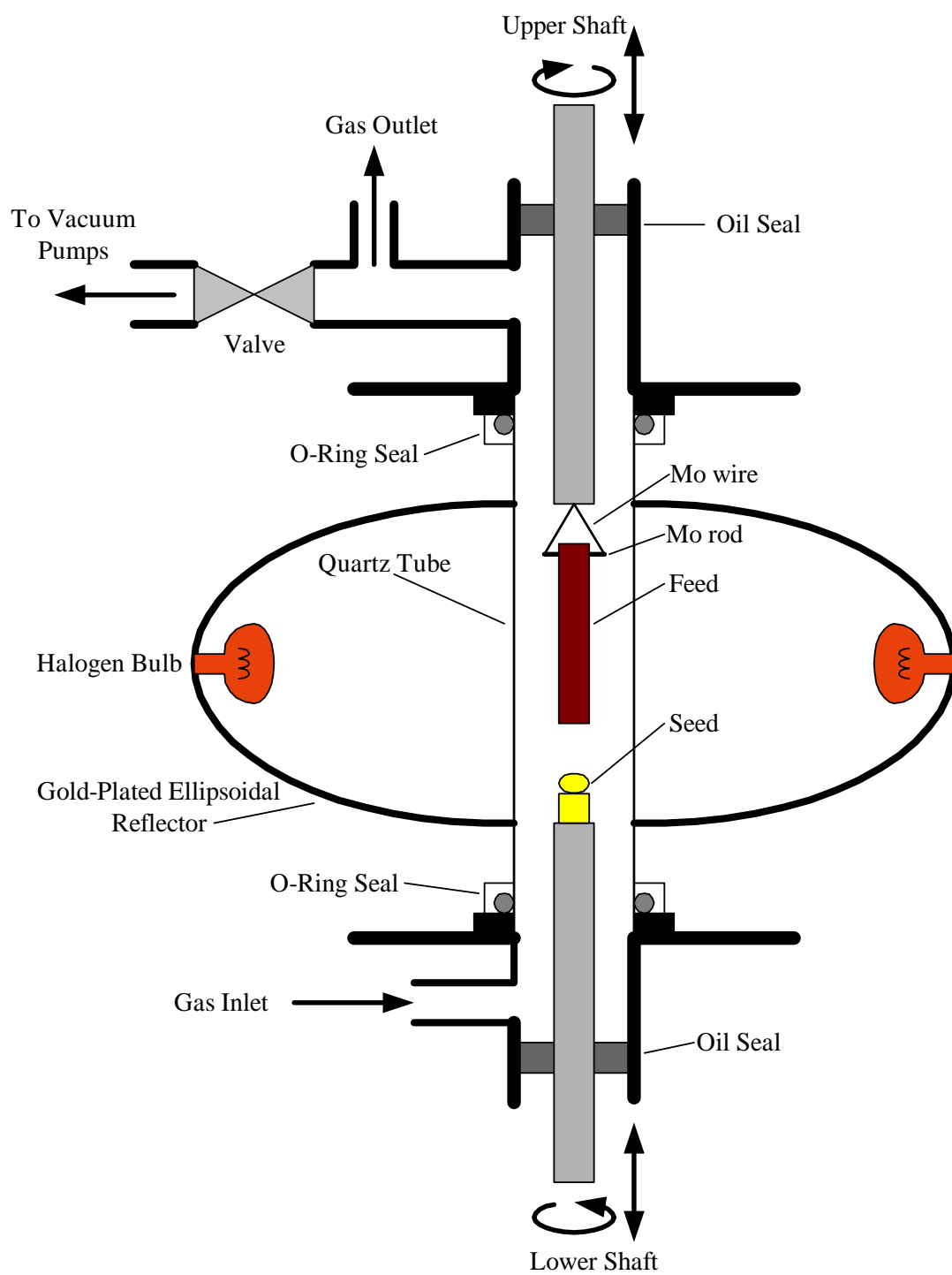

Figure 2.1 Schematic diagram of the NEC SCN35HD Image Furnace.

Initially, a molten zone is formed when the tip of the seed and the feed bar are brought close together at the foci of the ellipsoidal mirrors. The current to the halogen lamps is increased until the material melts and the two pieces become joined by a molten pool of material. The single crystal is produced by slowly pulling the seed away from the molten zone while the feed bar is lowered into the zone. Molten material attached to the seed solidifies as heat is lost through conduction into the lower shaft and by radiation. The feed and seed are rotated in opposite directions so that the molten zone is evenly heated, although the rotation acts to stir and homogenize the liquid. The rates at which the two shafts are moved can be reduced to less than 1 mm/hr and can be independently controlled. The machine can be used for reshaping an ingot or even growing long thin crystals from relatively short, even irregular lumps of material. By simple measurement of the profile of the feed ingot before loading the furnace, and elementary calculation, a skilled operator is able to pull out long and uniform crystal by making gradual changes in the pulling rate which is monitored and displayed digitally.

To ensure that the solid-liquid interface moves at the same speed as the lower shaft and the heat flow in and out of molten zone remains in equilibrium, the length of the molten zone is monitored using a video camera. A graduated scale visible on the monitor enables precise determination of the zone length.

Single crystal was grown in an atmosphere of purified Ar gas. Before purging with Ar, the grown chamber was pumped down to 1×10^{-6} mbar to remove as much oxygen as possible. Two inert gas purification units operating in parallel reduce the oxygen content of the Ar to very low levels. After the Ar has flowed through the chamber, it exits the system via a simple airlock to prevent back diffusion of oxygen.

Flow of gas is essential to prevent the build up of evaporation on the quartz tube in the region of the molten zone, which would restrict heating.

2.2 Preparation of thin foils and chemical analysis

After crystal growth, both TEM and SEM samples (~0.6 mm thick) were cut perpendicular to the crystal rod using a wire cut machine. To make TEM samples, a disc was glued on a Gatan disc grinder using superglue. After about 30 minutes the sample was ground on silicon carbide papers using the paper grades 500, 1000 and 1200, respectively, to produce disc ~0.3 mm thick. To take the sample out, the glue was dissolved by immersion in acetone. The smooth surface of the sample was then glued on the disc grinder and ground to the thickness of about 0.1 mm. A few TEM samples with 3 mm diameter could be cut from each disc using a Gatan ultrasonic disc cutter. Final thinning was done in a tenupol apparatus using 20% nitric acid in methanol as an electrolyte at temperatures between –20 and – 40°C and 12 volts potential.

For each optical and SEM sample, a disc was mounted into a conductive substance and then ground on fine silicon carbide papers following by grinding on Md-Nap paper using alumina past with the grain size reduce from 1.0, 0.3 and 0.05 µm, respectively. After optical and SEM observations, the samples were used for chemical analysis.

2.3 Characterization

After crystal growth, the Laue X-ray method was used to check the axial direction of the rod crystal. A BRUKER X-ray Diffractometer D5005 was used to

study the structure of the crystal. The microstructure of the crystal was studied using optical, scanning and transmission electron microscopes.

Optical microscopy study was carried out using an Olympus microscope with Normarski interference contrast. Microstructures of the samples were characterized using a JEOL 2010 and a Philips CM200 transmission electron microscopes operating at 200 kV and fitted with a goniometer stage capable of tilting a sample ±60° in any direction. Hitachi S4500 and JSM6400 scanning electron microscopes were used also.

The chemical compositions of the matrix were measured using WDS technique. A Cameca SX50 microprobe analyzer was used with a beam size of 0.7 μm and a step size of 0.5 μm.

2.4 Disordering experiment

Disordering of the alloy due to a mechanical milling process was studied. A stainless steel vial with an inside diameter of 46 mm and a hard steel ball of 10 mm diameter were used. About 5 g of the crystal was crushed into powder particles in the ball mill. An X-ray diffractometer was used for structural characterization after milling for 10 minutes up to 15 hours. Usually ball milling causes the temperature to increase and if the temperature gets too high the machine automatically stops. For milling times of 1 hour and longer, milling had to stop every 30 minutes to let the temperature low down and re-starting the milling process again after 30 minutes.

CHAPTER III

EXPERIMENTAL RESULTS

3.1 Single crystal of Ti-Al-Mn alloy

Figure 3.1 shows the NEC SCN35HD Image Furnace machine used to grow single crystals of Ti-Al-Mn alloy. Figure 3.2 shows the feed material after arc-melting. One end of the feeding rod was spark-drilled to make a hole for the insertion of a Mo rod as mentioned in Chapter II. Figure 3.3(a) shows the feed and seed materials, which are attached to upper and lower vertical shafts respectively. In this study the feed and seed materials were rotated in the opposite direction so that the molten zone is evenly heated at the rate of 8 rpm and at the pulling rate of 6 mm/h. Since the diameters of the feed material was not uniform and also bigger than the seed, the feeding was done at a very slow rate and required adjustments in order to keep the solid-liquid interface moving at the same speed. At the end of growing process, the feeding material and the crystal were melted apart from each other as can be seen in Fig. 3.3(b). Figure 3.4 shows the as-grown crystal, which has a rod shape of 6 mm in diameter and 130 mm long. Note that the seed crystal is on the right side in the picture.

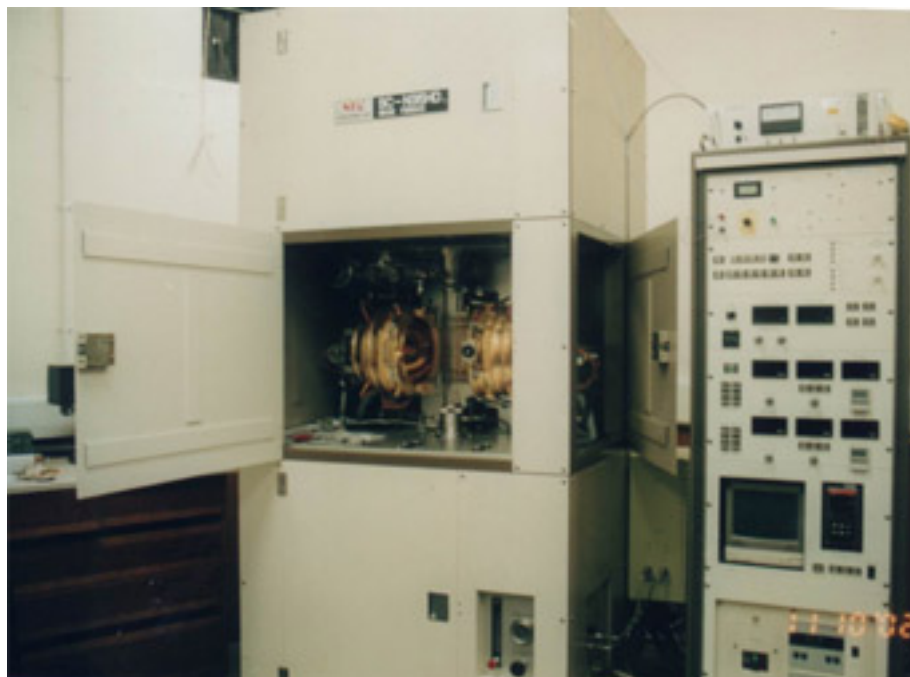Figure 3.1 The NEC SCN35HD Image Furnace machine.

a spark-drilled hole
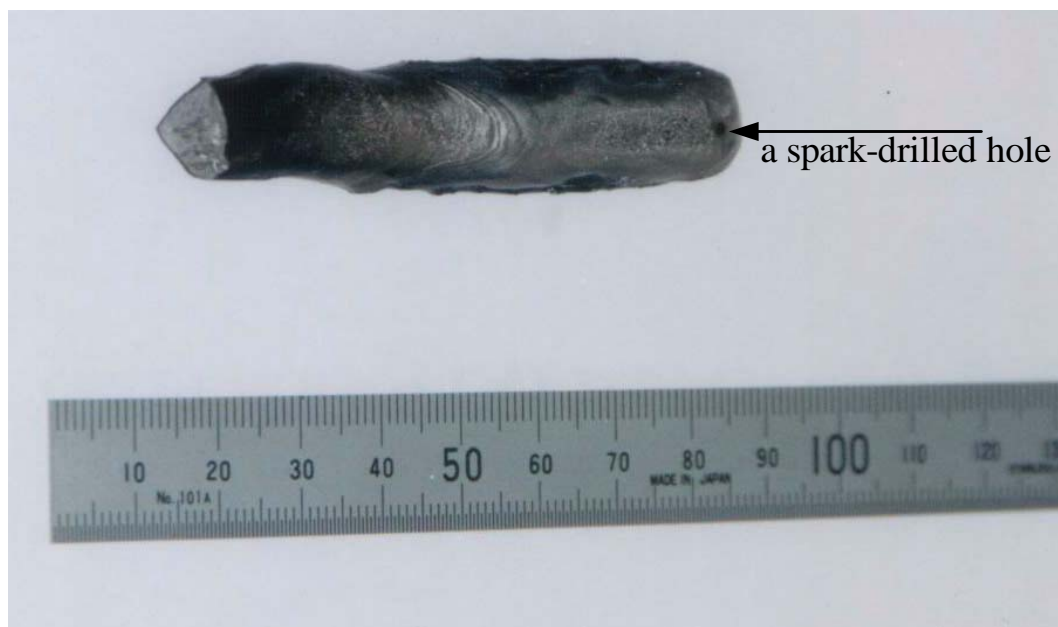
Figure 3.2 The feed material after arc-melting.
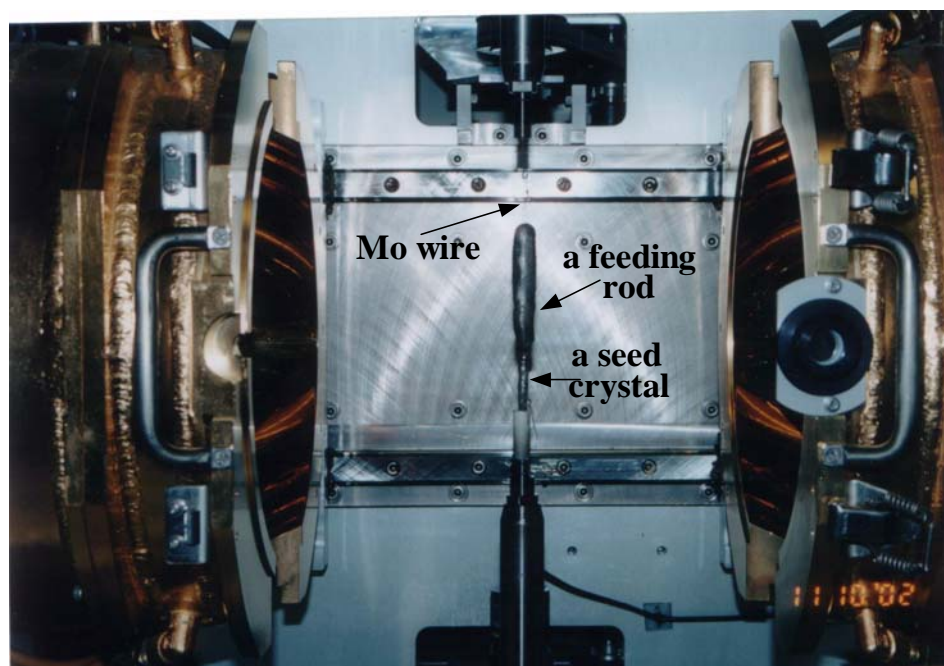
(a)
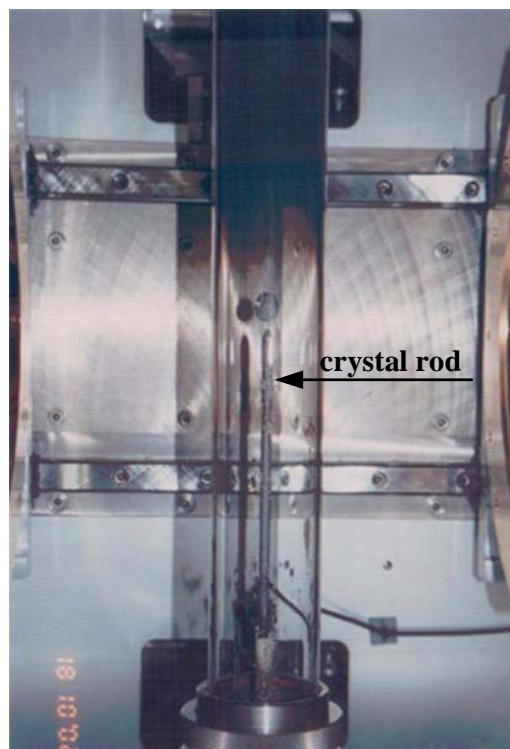
(b)

Figure 3.3 (a) The positions of the feed and seed materials in the crystal growth machine.

(b) The rod crystal after growth.
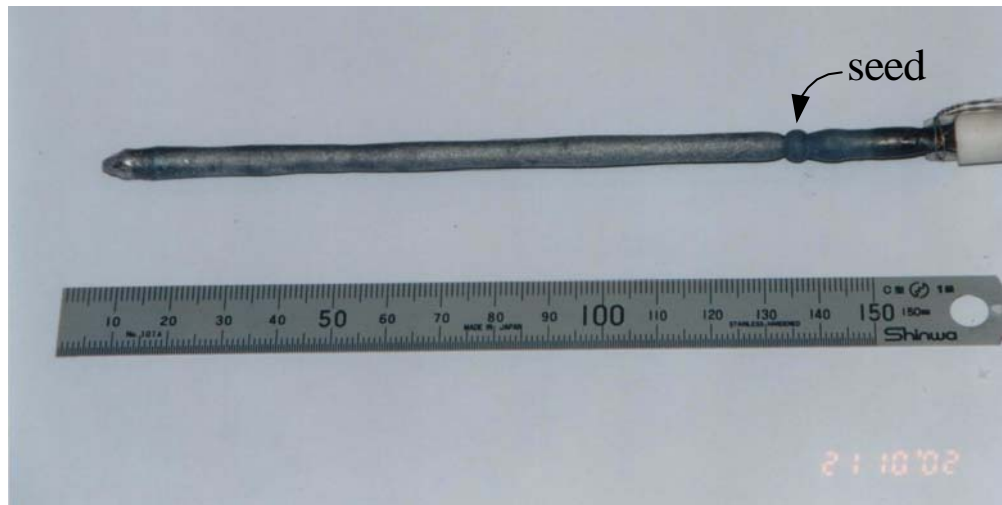
Figure 3.4 The as-grown crystal.

Figure 3.5 shows the diagram of the X-ray Laue method used to determine the crystal orientations. The result from X-ray Laue photographs are shown in Fig. 3.6(a), which shows that the rod was a single crystal after growth. A stereographic projection analysis shows that its axial orientation is close to the [100] direction in a standard reference triangle as shown in Fig. 3.5(b).

Figure 3.5 The diagram of the X-ray Laue method.
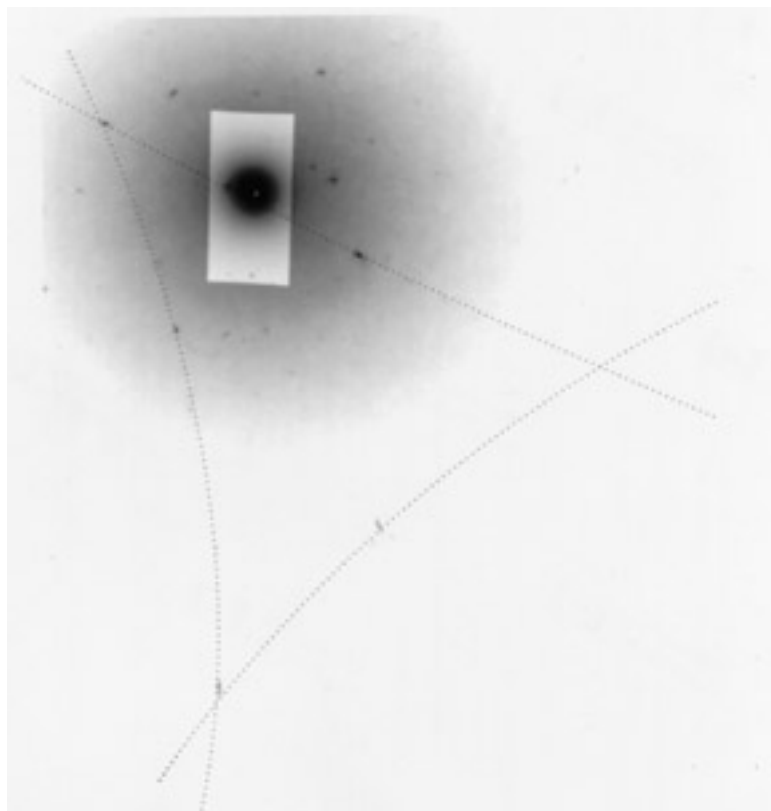
(a)
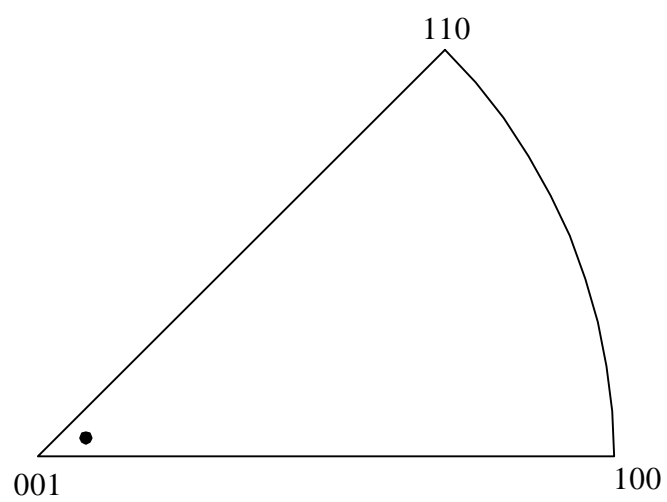
(b)

Figure 3.6 (a) X-ray Laue photograph of the material.

(b) Orientation of the crystal in a standard reference triangle.

3.2 Sample preparation and chemical analysis

Figure 3.7 shows the samples cut from the rod crystal using a wire-cut machine. Some samples were broken, as indicated by the arrows in the figure, during the cutting process due to brittleness. Therefore, the condition for cutting, such as the speed and current had to be optimized to minimize the breaking of the samples. These discs were there used to make specimens for the microscopy studies and c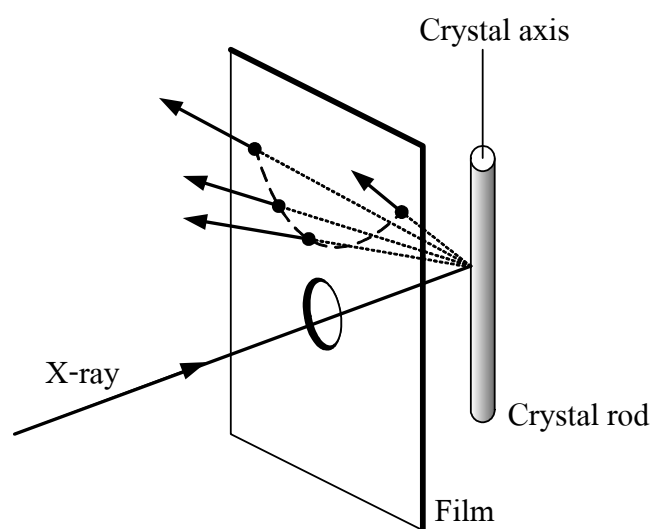hemical analysis. Figure 3.8 shows an example of the specimens used for optical and scanning electron microscopy studies.
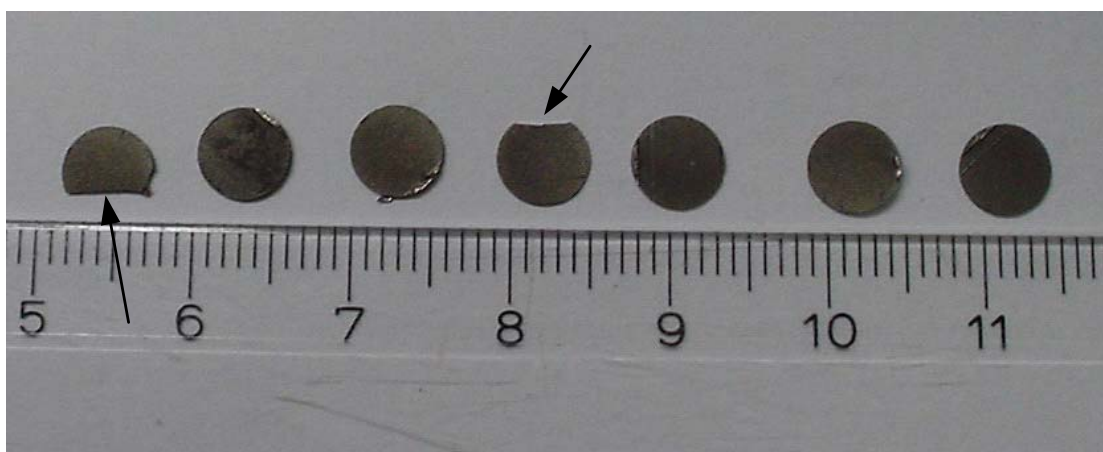
Figure 3.7 Samples from the as-grown crystal.

Table 3.1 shows the chemical contents of the crystal measured by the Camica SX50 microprobe analyzer. Twelve values of Ti, Al and Mn contents in atomic percent unit were measured over the cross-sectional area of one sample. Similar results were obtained using different specimens. The average contents are 67.3, 26.5 and 6.2 atomic percents for Al, Ti and Mn respectively.
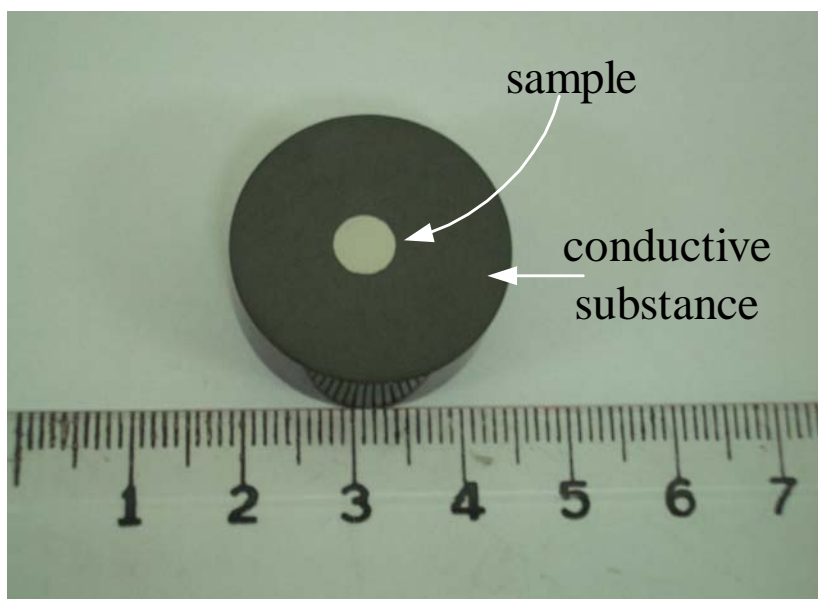
Figure 3.8 Optical and SEM specimen.

Table 3.1 Chemical compositions of the crystal.

	Atomic percent		
No.	**Al**	**Ti**	**Mn**
1	67.13	26.56	6.32
2	67.00	26.67	6.33
3	67.19	26.82	6.00
4	67.31	26.61	6.08
5	67.15	26.51	6.34
6	67.31	26.39	6.30
7	67.11	26.69	6.20
8	67.29	26.48	6.23
9	67.37	26.57	6.07
10	67.66	26.38	6.97
11	67.29	26.35	6.36
12	67.34	26.46	6.21
Average	**67.26**	**26.54**	**6.20**

3.3 Characterization

3.3.1 X-ray diffraction

The BRUKER X-ray diffractometer model D 5005 with wave length 1.54 Å was used to study the structure of the crystal. Figure 3.9 shows the diffracted peaks from powder sample. After some analysis, the plane index (h k l) that corresponds to each peak in the XRD pattern can be found.

Figure 3.9 The XRD pattern of sample.

The procedure to obtain (h k l) is summarized in table 3.2(a). Table 3.2(b) shows a few plane indices that do not give zero structure factor for f.c.c. lattice (Kittle, 1991).

Table 3.2 (a) The samples of the indices of f.c.c. lattice, which provide non zero structure factor.

(h k l)	$h^2 + k^2 + l^2$
(111)	3
(200)	4
(220)	8
(222)	12
(311)	11
(331)	19
(333)	27

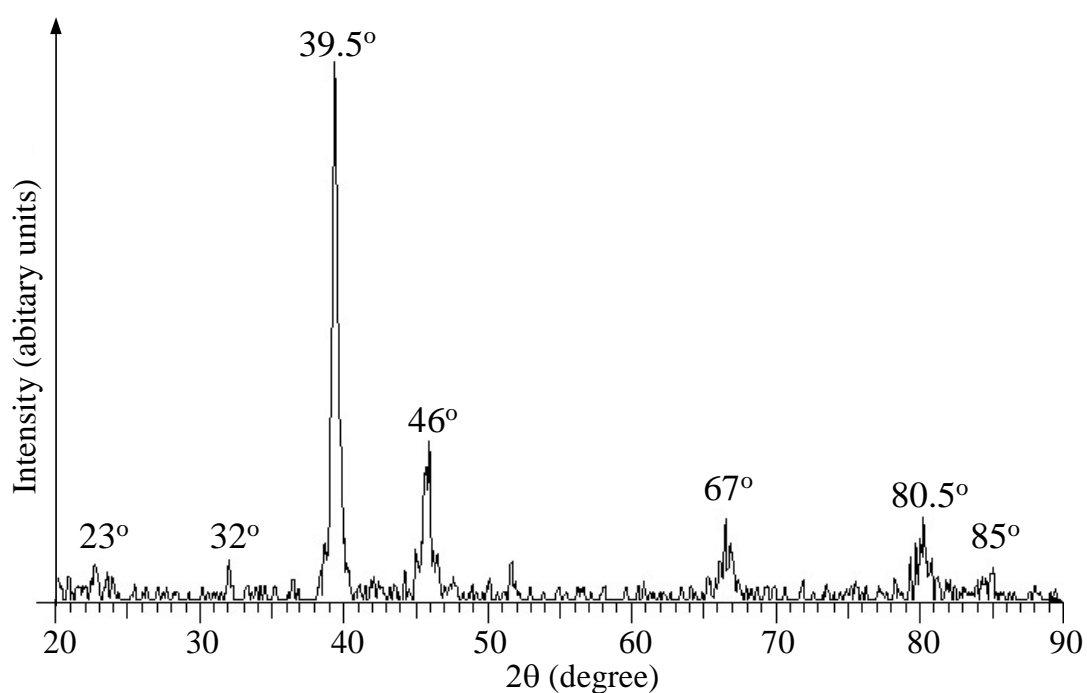(b) The summary of the procedure used for calculate (h k l) from Bragg law $2d_{hkl} \sin\theta = n\lambda$, and $d_{hkl} = \dfrac{a}{\sqrt{h^2 + k^2 + l^2}}$.

Peak No.	2θ	$\sin^2\theta$	$\dfrac{\sin^2\theta}{0.114}$	$\dfrac{\sin^2\theta}{0.114} \times 3^*$	$h^2 + k^2 + l^2$	(h k l)
1	39.5°	0.114	1.00	3	3	(111)
2	46°	0.153	1.034	4.04	4	(200)
3	67°	0.305	2.068	8.04	8	(220)
4	80.5°	0.417	3.066	10.98	11	(311)
5	85°	0.456	4.00	12	12	(222)

* Note that other numbers cannot provide sensible $h^2 + k^2 + l^2$.

Figure 3.10 shows the X-ray diffraction pattern of the crystal with the plane indices. The pattern shows the Bragg peaks (111), (200), (220), (311) and (222) as the evidence of the f.c.c. structure. A superlattice peaks (100) and (110) relatively low in intensity, are also visible. This X-ray spectrum together with the TEM diffraction pattern, which is described in the next section, indicate that the cubic titanium trialuminide has an ordered $L1_2$ structure. There is no clear peak arising from other phases. As can be seen in the SEM micrograph, the matrix contains no dendritic structure of the second phase as found by Manyum and Taylor (2002). Although TEM results show that the matrix contains fine precipitate particles of $TiAl_2$ (Ga_2Hf type structure), their volume fraction is very small. The figure suggests that there may be a small peak of the second phase at 2θ around 67, 80 and 85 degrees. However, X-ray diffraction investigation around these areas still shows no clear peak of the second phase as can be seen in Fig. 3.11. The lattice parameter calculated from

$$a_{hkl} = \frac{n\lambda\sqrt{h^2 + k^2 + l^2}}{2\sin\theta}$$, with λ = 1.54 Å and n = 1, is 3.947 Å as seen in Table 3.3. An example of the $L1_2$ matrix containing second phase of $D0_{22}$ structure can be seen in the study of " Disordering and reordering of an $TiAl_3$-Mn-Nb alloy" by Che, Wang, and Hu (1995) as shown in Fig.3.12.
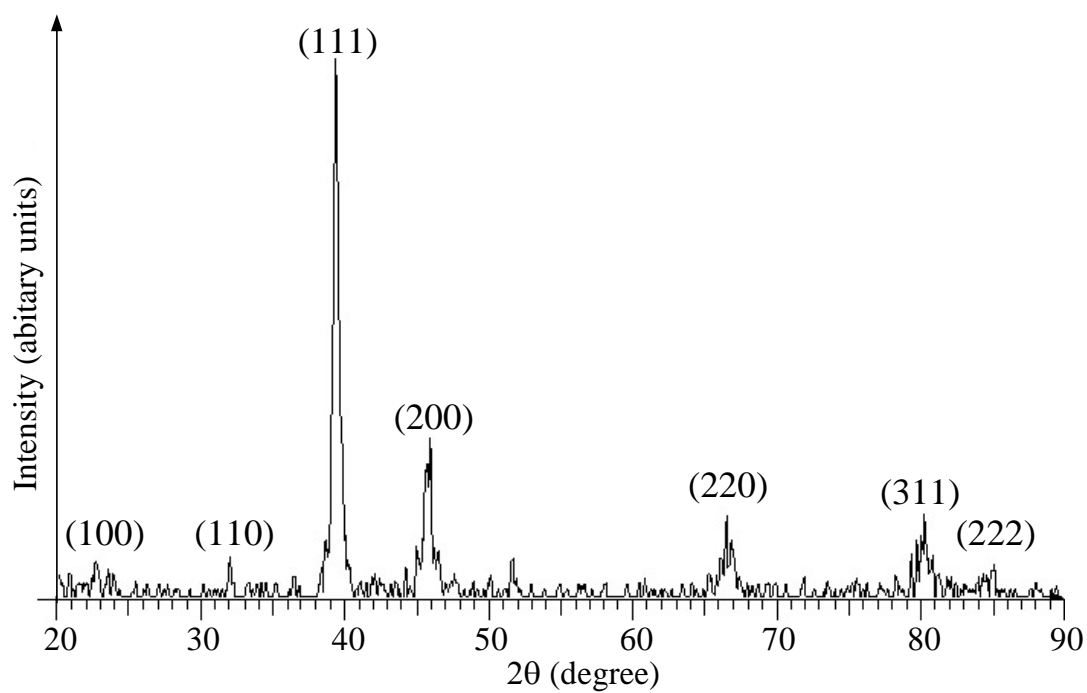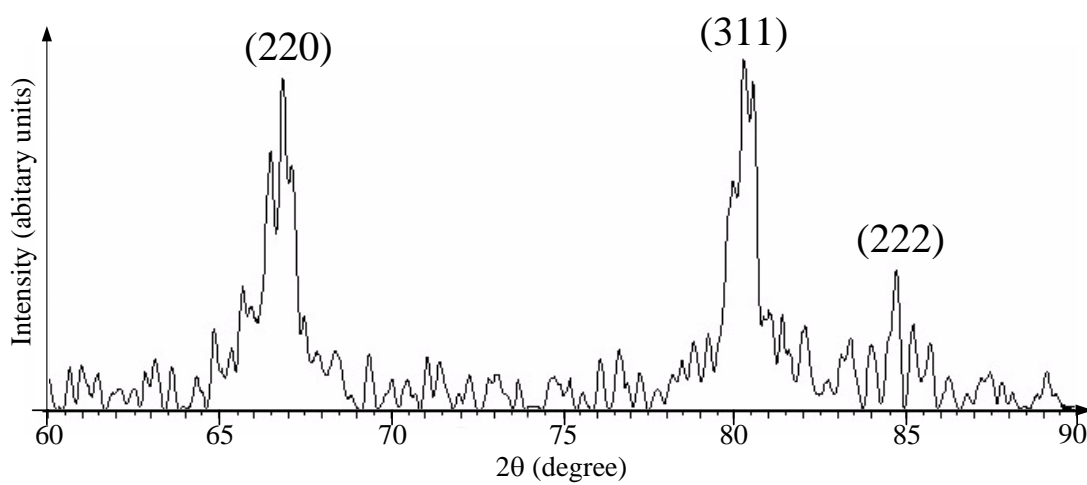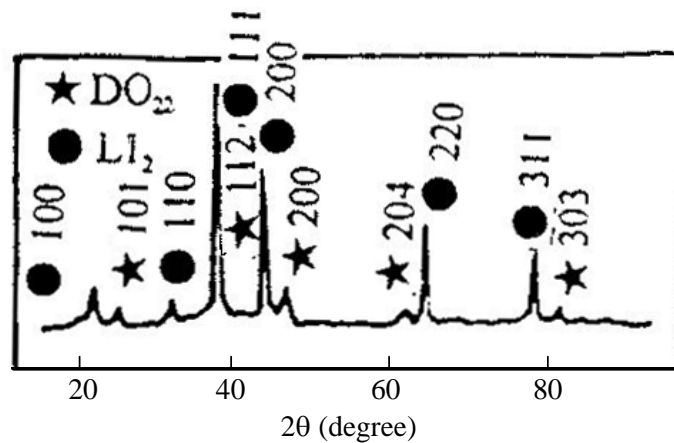
Figure 3.10 X-ray diffraction pattern of the crystal.

Figure 3.11 X-ray diffraction pattern around $2\theta = 67^{o}$, 80° and 85°

Table 3.3 The summary of the calculation of the lattice parameter for the XRD peaks.

Peak No.	(h k l)	2θ	θ	$a_{hkl} = \dfrac{n\lambda\sqrt{h^2+k^2+l^2}}{2\sin\theta}$ (Å)
1	(111)	39.5°	19.75°	3.947
2	(200)	46°	23°	3.941
3	(220)	67°	33.5°	3.946
4	(311)	80.5°	40.25°	3.952
5	(222)	85°	42.5°	3.948
			Average	3.947 ± 0.004

Figure 3.12 The XRD pattern of $L1_2$ and $D0_{22}$ phases (Che et al. (1995)).

3.3.2 Optical and scanning electron microscopy

No second phase was found under the optical investigation. However, some cracks and pores were observed as seen in Fig. 3.13. The optical micrograph shows the trails of cracks joint between pores. It is difficult to determine when these cracks occurred during the process. They might be created during crystal growth due to the solidification process or, they might occur during the specimen preparation.

Figure 3.14 shows a typical SEM micrograph of the single crystal. Since the SEM specimens were cut perpendicular to the rod crystal, different areas across the rod crystal can be observed. No second phase precipitates were observed using SEM. Again, pores were observed also, but their volume fraction was small.
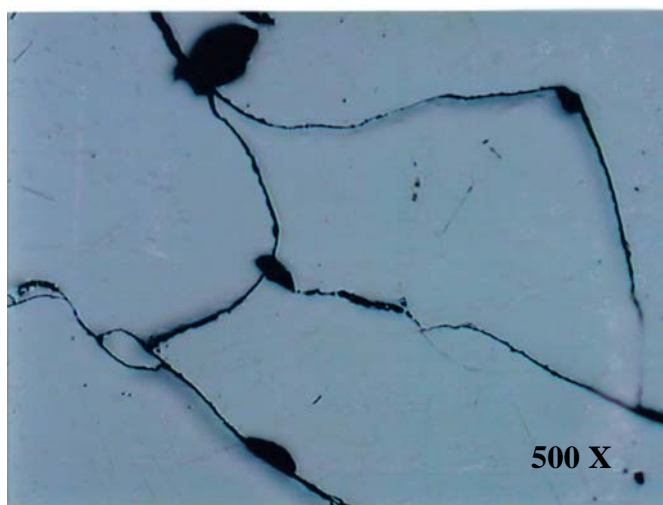

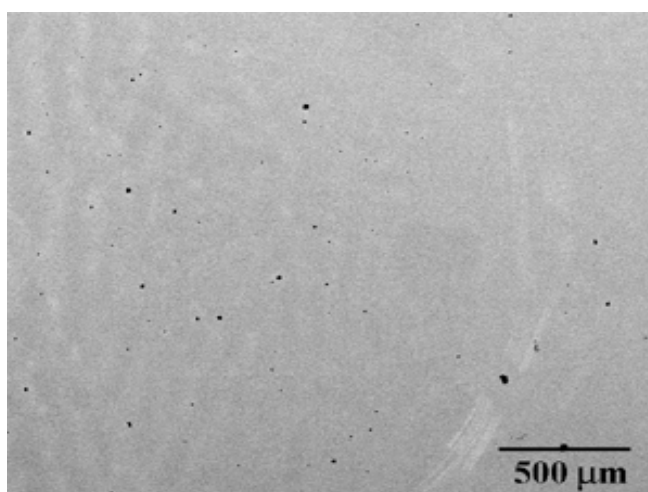Figure 3.13 Optical micrograph showing trails of cracks joining between pores.

Figure 3.14 A typical SEM micrograph showing pores.

3.3.3 Transmission electron microscopy

TEM examination also shows that the crystal has a cubic $L1_2$ structure. Figure 3.15 shows a selected area diffraction (SAD) pattern taken from a TEM specimen prepared as described in Chapter II along the [001] zone axis. The planes to diffract from the crystal must be perpendicular to the zone axis. This pattern is diffracted from an f.c.c. single crystal.
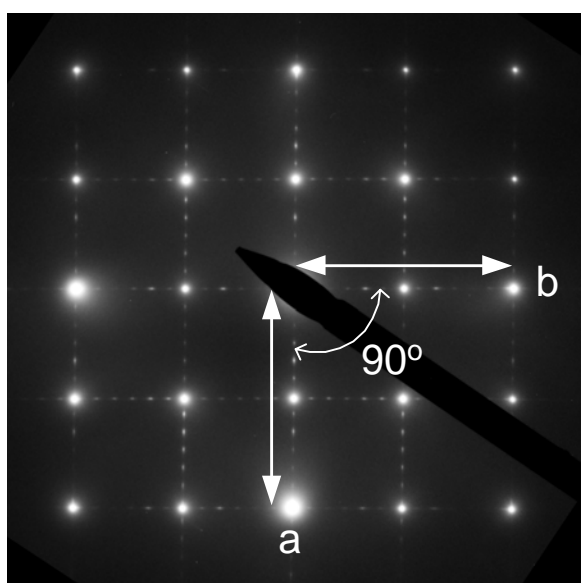
Figure 3.15 A selected area diffraction pattern along the [001] zone axis.

From the diffraction pattern, the spots form a square lattice. The ratio of the principal spot spacing is defined as the ratio of the distance to the two nearest diffraction spots in different directions, in this case a and b, the ratio of this pattern is 1:1 and the angle between them is 90°. From the table, we see that this means the zone axis is the [100] system.

The zone axis was specified further after indexing the spots. For an f.c.c. crystal, mixing of even and odd is not allowed by considering the structure factor but might be due to supperlattice diffractions. The allowed diffraction spots must be

perpendicular to the zone axis [001] so that

$$[h\,k\,l] \cdot [001] \;=\; 0\,.$$

By using the transmission spot [000]. The spots that could be consistent are:

$[100] \cdot [001] \;=\; 0$ $\qquad\qquad\qquad$ $[010] \cdot [001] \;=\; 0$

$[200] \cdot [001] \;=\; 0$ $\qquad\qquad\qquad$ $[020] \cdot [001] \;=\; 0$

$[\bar{2}00] \cdot [001] \;=\; 0$ $\qquad\qquad\qquad$ $[0\bar{2}0] \cdot [001] \;=\; 0$

$[110] \cdot [001] \;=\; 0$ $\qquad\qquad\qquad$ $[220] \cdot [001] \;=\; 0$ $\quad$ etc.

The spots [100] and [010] are lowest order and should be chosen to index the principal spots unless the diffraction pattern has supperlattice spots in which case the [200] and [020] should be chosen for the principal spots instead. Because a and b make a right angle then the next step is to check the angle between the planes. The dot produce of two normalized vectors equals the cosine of the angle between them. To normalize vectors we multiply by the factor $1/\sqrt{h^2 + k^2 + l^2}$.

$$\frac{1}{2}[200] \cdot \frac{1}{2}[020] \;=\; 0 \;=\; \cos\theta$$

So θ is 90°. The indexing of a diffraction pattern must also satisfy the right hand rule, where the zone axis is toward to the electron gun, therefore the spot at a is [200] and that at b is [020].

The supperlattice spots between [200] with [000] and [020] with [000] are [100] and [010] respectively.

For indexing another principal spot the value h increases by 2 with each step down the column from [000] and decreases by 2 with each step up the column from [000] while k increases by 2 with each step rightward along the row from [000] and decreases by 2 with each step leftward along the row from [000] and the last indices in (h k l) are 0.

Figure 3.16(a) shows an indexed selected area diffraction pattern. Figure 3.16(b) shows a bright field (BF) image corresponding to Fig. 3.16(a). The SAD pattern is the superimposed reciprocal lattice of the matrix and the two orthogonal sets of precipitates. The SAD pattern of the matrix is consistent with the [001] zone of the f.c.c. structure. The fundamental reflections are indexed. The positions of the spots for the ordered $L1_2$-$TiAl_3$ unit cell are indexed in the lower left quadrant of the pattern. A few diffraction spots from precipitate are indexed in the top right quadrant of the pattern.

The two orthogonal satellite spots in Fig. 3.16(a) observed parallel to the <100> directions are the diffraction spots from the precipitates. These are $TiAl_2$ precipitates usually found in $L1_2$-$TiAl_3$ alloys. Wu and Pope (1994) have studied in the $TiAl_2$ phase using Fe- and Cr-stabilized $L1_2$-$TiAl_3$ single crystals. It has a tetragonal structure of the Ga_2Hf type structure. The structural relationships between the precipitates and the matrix together with the effects of the precipitates on the mechanical property of the alloys were reported. Similar TEM results were obtained by Potez, Lapasset, and Kubin (1992), in Cu-modified $L1_2$-$TiAl_3$ and by Tian and Nemoto (1997, 2000a, 2000b) in Ag-modified $L1_2$-$TiAl_3$. They found from the study of electron diffraction patterns that the orientation relationship between the precipitates and the matrix can be described as

$$(001)_p//(001)_m, [100]_p//[100]_m \text{ and plate}//\{100\},$$

where m and p denote the matrix and precipitate, respectively.
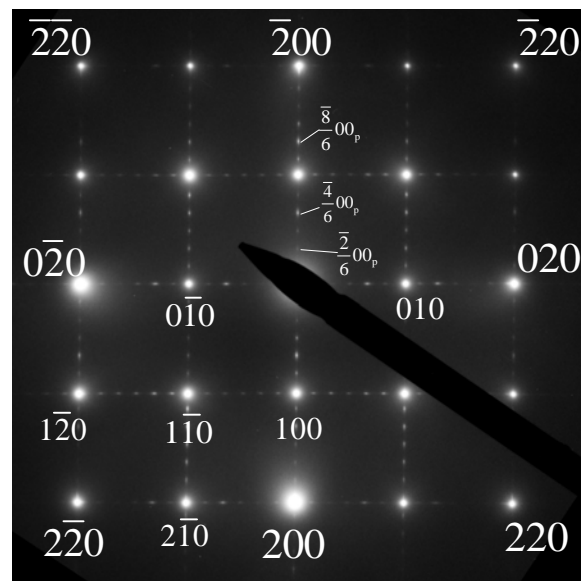
(a)
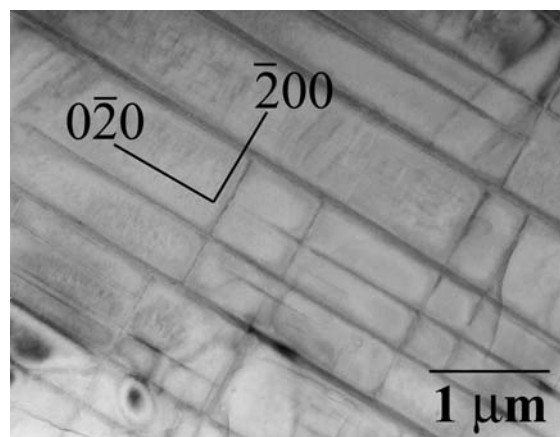
(b)

Figure 3.16 (a) SAD pattern of the matrix and precipitates. The zone axis of the

matrix is [001].

(b) A BF image of the area used to obtain the SAD pattern in (a),

B = [001].

Figures 3.17(a) and (b) show the crystal structure of the $L1_2$-$TiAl_3$ and $TiAl_2$, respectively. The $TiAl_2$ structure can be derived from the $L1_2$ structure by a combination of translations of the {100} planes along one of the cube edges. By doing this, we can modify the stacking sequence of the {100} planes of the $L1_2$ structure from alternating mixed planes having the composition of TiAl and pure Al planes, TiAl/Al, into pairs of mixed planes alternating with a pure Al plane, TiAl/TiAl/Al.

It can be seen in Fig. 3.16(b) that $TiAl_2$ precipitates about 0.1 μm thick lie parallel to the (100) and (010) cube planes of the matrix. Figure 3.18(a) shows a dark field (DF) image from a diffraction spot of the $TiAl_2$ precipitates. Figure 3.18(b) shows the condition of SAD pattern near the [001] zone axis and the diffraction spot, indicated by an arrow next to the 100 superlattice reflection spot from the matrix, used to obtained the DF image in Fig. 3.18(a). Fringes can be seen, for example, at A. These fringes show the antiphase domain boundary of the precipitates since the image was obtained from the spot arises from ordering structure of the precipitates. These fringes are called π fringes which give symmetric fringes in DF and BF and complementary BF/DF pairs.

Figure 3.19 shows a higher magnification of the precipitates. This is a BF image obtained near the [001] zone axis. Two features were observed in these precipitates. Firstly, there were steps on some of the precipitates, see for example at A These steps probably occurred when the plate precipitates continued to grow thicker on the {100} cube planes of the matrix. The other feature observed was that some of these precipitates can continue to grow into other precipitates that lie on other {100} planes of the matrix, see for examples at B. However, usually, these precipitates seem to stop growing when they reach another precipitate as can be seen at C. The fringes

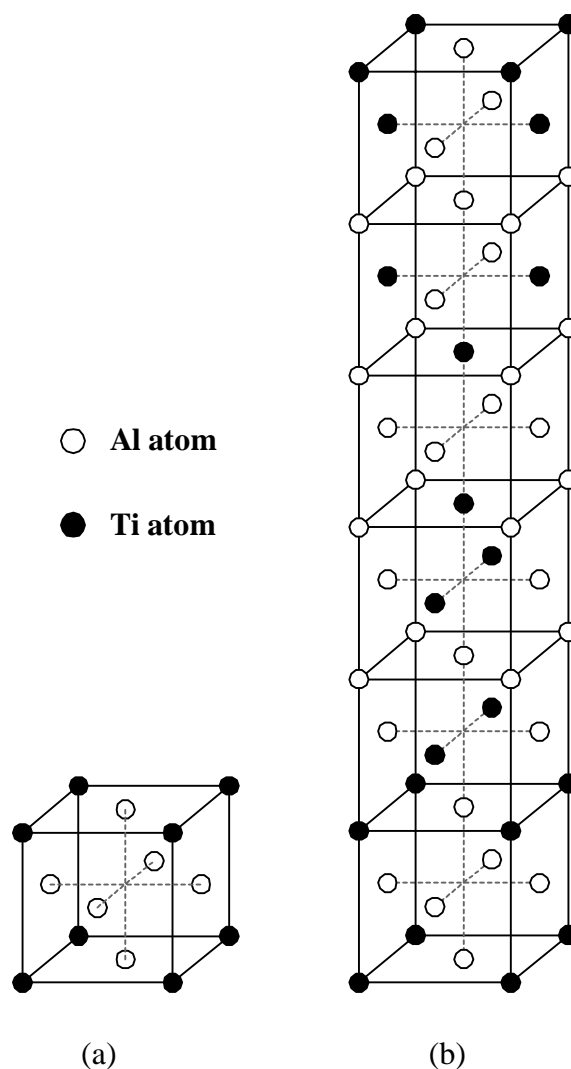observed are again due to the order structure of the precipitates.

Figure 3.17 Crystal structures of (a) $L1_2$-$TiAl_3$ and (b) $TiAl_2$ (Ga_2Hf type).

Some area between the precipitates in Fig. 3.16(b) seems to be empty, however, it actually contains fine precipitates as seen in Fig. 3.20(a). This TEM image looks like a BF image but is in fact a DF image taken from three diffraction spots near the [011] zone axis as indicated in the SAD pattern in Fig. 3.20(b). The three spots consist of a (100) spot from the matrix and two spots from the precipitates that are on both sides of the matrix spot.
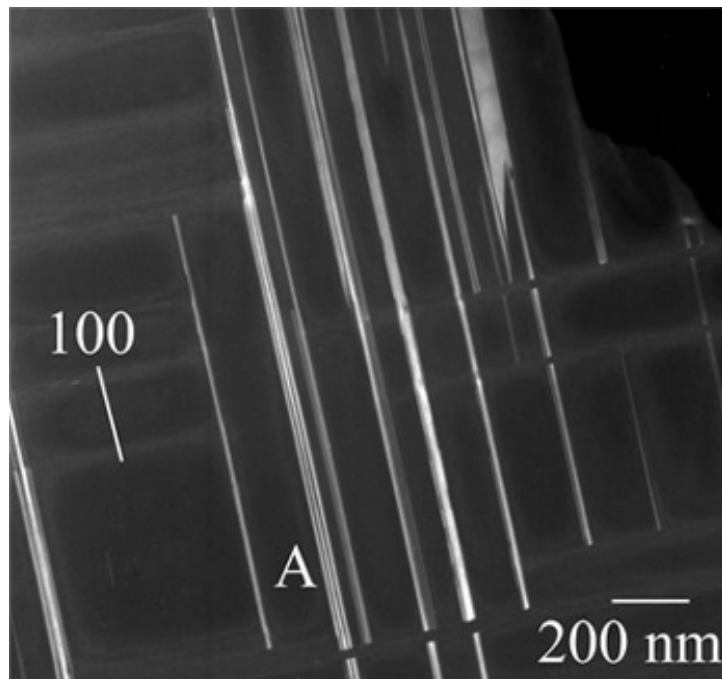
(a)
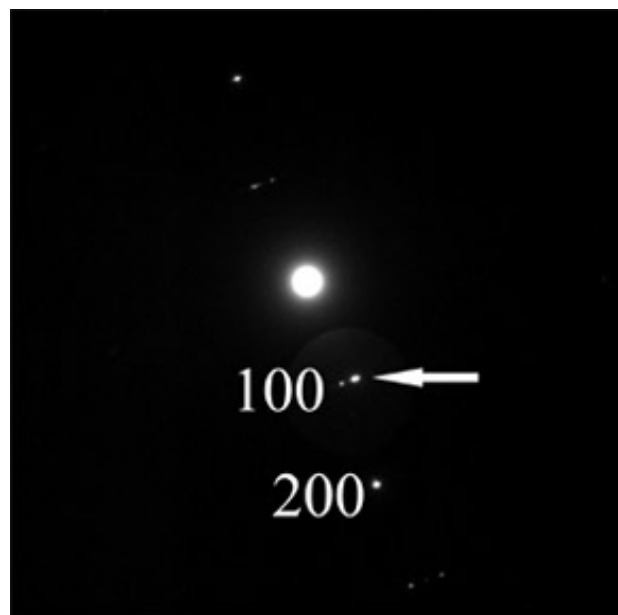
(b)

Figure 3.18 (a) A DF image showing TiAl$_2$ precipitates, B = [001].

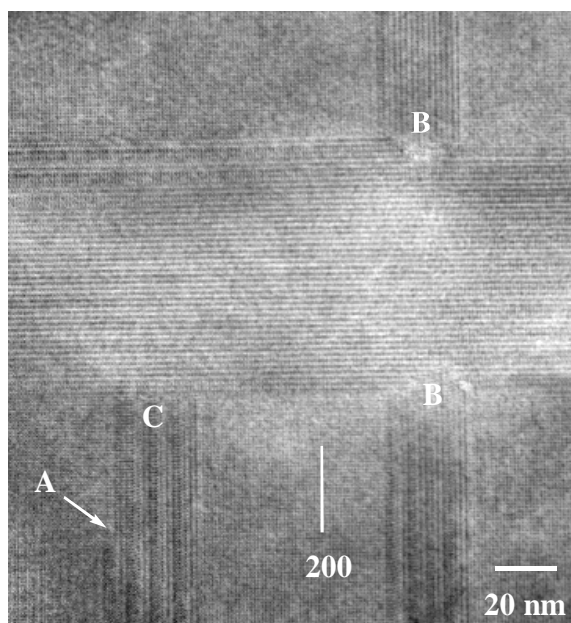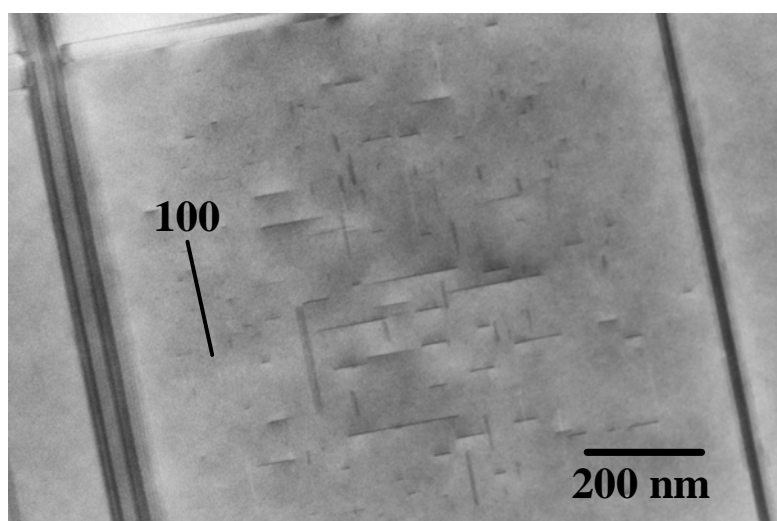(b) A SAD pattern and the diffraction spots used to obtain the image

in (a).

Figure 3.19 TEM BF image showing a higher magnification of Fig. 3.18(a)

(a)

Figure 3.20 (a) A DF image showing fine precipitates.
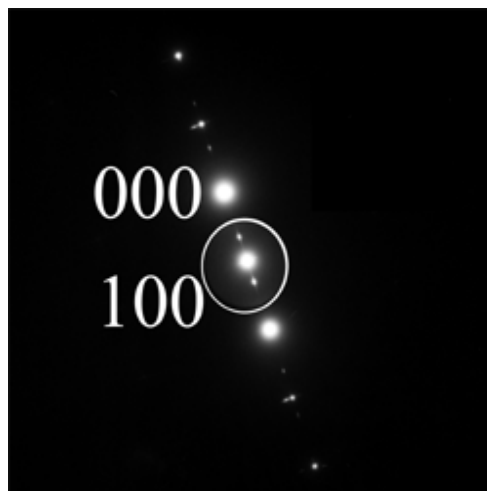
(b)

Figure 3.20 (b) SAD pattern and diffraction spots used to obtain the image

in (a).

3.4 Disordering of the compound

Figure 3.21 shows the X-ray diffraction spectra obtained from the powder of the crystal after ball milling for 10 min, 1 h, 5 h and 15 h, respectively. It can be seen that the (111), (200), (220) and (311) fundamental peaks of the f.c.c. lattice broaden and decrease in intensity as the milling time increases. The low intensity superlattice (100) and (110) peaks become invisible after 5 h milling which means that the matrix becomes disordering. After 15 h milling the powder material becomes almost amorphous.

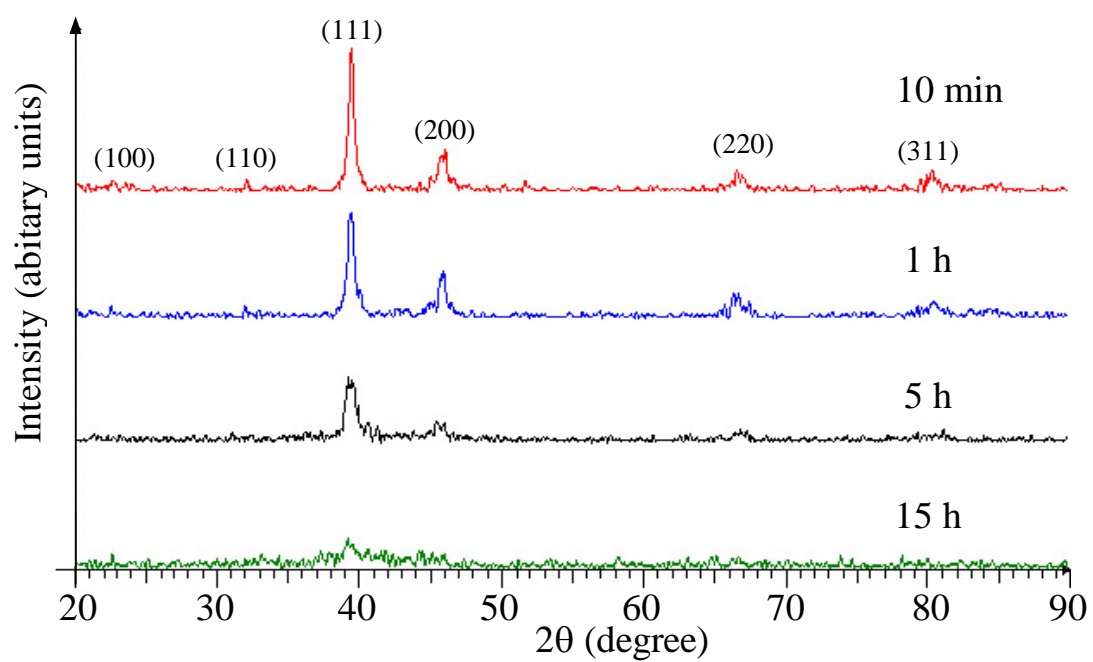Figure 3.21 X-ray diffraction patterns after milling for difference period of time.

CHAPTER IV

DISCUSSION AND CONCLUSIONS

Most experimental techniques were carried out using conventional methods. However, although crystal growth was carried out using the commercial machine, it is difficult to grow a long and uniform diameter crystal rod partly because the feeding material was not uniform. Fluctuations in the size of the molten zone can be caused by inhomogeneous feed material, with varying solute concentration leading to a variable melting point. The length of the feed bar also affects the zone size; as the feed bar is consumed, the surface area from which radiation of heat can occur is reduced. This results in an increase in temperature of the molten zone and an increase in zone length. To obtain a crystal of a uniform diameter, it is necessary to make adjustments in the rate at which the feed bar is lowered into the molten zone.

The results of X-ray diffraction pattern and TEM study confirm that the prepared material has an ordered $L1_2$ structure. Although only the superlattice (100) and (110) peaks with very low intensity were observed in the X-ray spectra, it is believed that if the experiment was carried out in an evacuated chamber, more superlattice peaks may be visible. This is because the background intensity is reduced due to air scattering on the beam path.

Although the crystal structure is changed from the tetragonal to cubic structures by alloying with Mn, the material is still very brittle, which means that other factor(s) other than its crystal structure control the brittle to ductile transformation.

From the SEM result, it is possible to eliminate the second phase with dendritic structure in the $L1_2$-$TiAl_3$ matrix by controlling the amount of the Mn concentration. However, it seems that the reduction of the second phase causes the porosity to increase in the matrix as seen in Fig. 3.14.

TEM observation shows fine precipitates of a plate-like of the $TiAl_2$ particles. This is not unexpected since $TiAl_2$ has a tetragonal structure of Ga_2Hf type which can be constructed from the f.c.c. lattice. The precipitation of $TiAl_2$ phase has been observed in most $L1_2$-$TiAl_3$ compounds stabilized with Fe, Cu, and Ag (Wu and Pope, 1994).

In the present work millings were carried out in the ambient pressure which means that oxidation may occur and other oxide second phases may form as the temperature increases during the milling process. However, the X-ray diffraction results show that no other second phase apart from the $L1_2$-$TiAl_3$ matrix phase was observed, even the spectrum of the $TiAl_2$ phase was not visible. If there was any oxide phases occurring during the process, their volume fraction must be very small and thus not in the visible in the X-ray diffraction patterns.

REFERENCES

REFERENCES

Bohnenkamp, U., Wang, G -X., Jeweet, T. J., and Dahms, M. (1994).
Intermetallics. 2: 275-283.

Che, X., Wang, Q., and Hu, G. (1995). **Chinese science bulletin.** 40: 2081-2084.

Cullity. B.D., and Stock, S.R. (2001). **Elements of x-ray diffraction.** (3rd ed).
New Jersey: Prentice Hall.

Douin, J., Sharvan Kumar, K., and Veyssiere, P. (1995). **Materials Science &
Engineering.** A (192/193): 2-96.

Fukunaka, K., Kolba, M., Yamada, K., and Miura, Y. (1997). **Materials Science &
Engineering.** A (234-236): 594-597.

Fultz, B., and Howe, J. (2001). **Transmission electron microscopy and
diffractometry of materials.** Germany: Springer.

Kittle, C. (1991). **Introduction to solid state physics** (6th ed.). Singapore: Wiley.

Kogachi, M.,and Kameyama, A. (1995). **Intermetallics.** 3: 327-334.

Loretto, M.H. (1994), **Electron beam analysis of materials.** (2nd ed.). University
Press, Cambridge, Great Britain: Chapman & Hall.

Mabuchi, H., Kito, A., Nakamoto, H., Tsuda, H. and Nakayama, Y. (1996).
Intermetallics. 4: s193-s199.

Manyum, P., and Taylor, G. (2002). **Suranaree Journal of Science and Technology.**
7: 142-148.

Miida, R. (1986). **Japanese Journal of Applied Physics.** 25: 1815-1824.

Nakayama, Y., and Mabuchi, H. (1993). **Intermetallics.** 1: 41-48.

Nic, J. P., and Mikkola, D. E. (1999). **Intermetallics.** 7: 39-47.

Pettifor, D. G. (1993). **Materials science and technology** (Vols.1., pp.61-122). Germany: VCH.

Potez, L., Lapasset, G., and Kubin, L. P. (1992) **Scipta Metallurgica et Meterialia.** 26: 841-846.

Sauthoff, G. (1995). **Intermetallics.** Weinheim, New York: VCH.

Shirai, Y., Masaki, K., and Yamakuchi, M. (1994). **Intermetallics.** 2: 221-224.

Tian, W. H., and Nemoto, M. (1997). **Intermetallics.** 6: 193-200.

Tian, W. H., and Nemoto, M. (2000). **Intermetallics.** 8: 345-352.

Tian, W. H., and Nemoto, M. (2000). **Intermetallics.** 8: 835-843.

Varin, R. A., Wexler, D., Calka, A., and Zbroniec, L. (1998). **Intermetallics.** 6: 563-566.

Williams, D. B., and Carter, C. B. (1996). **Transmission electron microscopy: a textbook for materials science** (Vols. 1-4). New York: Plenum Press.

Wu, Z. L., and Pope, D. P. (1994). **Acta Metallurgica et Meterialia.** 42: 509-518.

CURRICULUM VITAE

Mr.Yutthapong Inkong was born in January 16th, 1971 in Udornthani province, Thailand. He obtained his B.Sc. in Physics from Ramkhamhang University in 1994. After that he worked as a researcher at the Material Properties Analysis and Development Centre, Thailand Institute of Scientific and Technological Research (TISTR). He then moved to work as a teaching assistance at the Institute of Science, Suranaree University of Technology from 1997 to 2001. From 2001 he became a M.Sc. degree student at the School of Physics, Institute of Science, Suranaree University of Technology.